ACS APPLIED MATERIALS & INTERFACES

Research Article

www.acsami.org

Layer-by-Layer Assembly of Polyelectrolyte Multilayers in Three-Dimensional Inverse Opal Structured Templates

Seon Ju Yeo,[†] Hyo Kang,[⊥] Young Hun Kim,[†] Sungsoo Han,[⊥] and Pil J. Yoo*[,†,‡]

[†]School of Chemical Engineering and [‡]SKKU Advanced Institute of Nanotechnology (SAINT), Sungkyunkwan University, Suwon 440-746, Republic of Korea

[⊥]Energy Laboratory, Samsung Advanced Institute of Technology (SAIT), Yongin 446-712, Republic of Korea

ABSTRACT: A novel means of layer-by-layer deposition (LbL) of polyelectrolyte multilayers on three-dimensionally porous inverse opal (3D-IO) structures is presented. The 3D-IO structures comprising UV-curable polymer are highly flexible and can be readily demonstrated as free-standing films with double-sided open porosity over a large scale. A conflict between the intrinsically hydrophobic polymeric structures and waterborne characteristics of the LbL deposition process is overcome by employing a mixed solvent system of water and alcohol. The deposition pH of the LbL assembly can strongly affect the charge density and the degree of entanglement of polyelectrolyte chains, resulting in contrastingly different film deposition and growth behaviors. Since this method utilizes a three-dimensionally structured surface as a deposition substrate, 3D-IO films with a thickness of tens of micrometers can be uniformly and completely deposited with polyelectrolyte multilayers using only several tens of bilayer depositions, which can offer a new pathway of fabricating functionalized polymeric films. Finally, the LbL treated 3D-IO films are applied to nanofiltration membranes for removing multivalent metallic cations. Due to the enhanced Donnan exclusion effect as a result of multiple interfaces formed inside the 3D-IO structures and the relatively large volumetric ratio of water-permeable polyelectrolyte complexes, outstanding membrane performance was observed. Specifically, a good rejection rate of metal ions was achieved even under highly diluted feed conditions without sacrificing the high permeation flux.

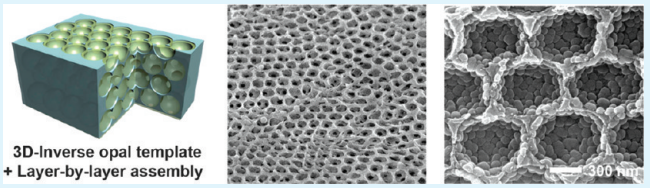

KEYWORDS: *polyelectrolyte multilayers, layer-by-layer assembly, inverse opal, porous structures, nanofiltration, membranes*

Layer-by-layer (LbL) deposition of polyelectrolyte multilayers has been extensively investigated during the last two decades as a beneficial means to create functionalized polymeric thin films with tunable physicochemical properties via manipulating various molecular interactions.[1,2] Since it requires an elaborate understanding and control over molecular interactions, it has received much interest as a fundamental topic of academic research. Indeed, due to the use of a dipping-based wet process and a readiness in scalability, LbL has been widely accepted for demonstrating industrial applications. Representative examples of relevance include functional surfaces,[2] optical films,[3−5] smart biomaterials,[6] hybridized electrodes for energy devices,[7] and next-generation electronic devices,[8] showing substantial potential for a variety of practical application areas.

In general, LbL deposition utilizes the alternately applied electrostatic binding interactions between cationic and anionic polyelectrolyte chains, forming an ionically complexed thin film on a flat substrate. The constructed films can be further transformed to porous structures or complexly shaped patterns through applying additional treatment or processing.[3,9] Moreover, by exploiting the LbL deposited polyelectrolyte thin films as a platform for self-assembly, various kinds of nanomaterials can be two-dimensionally assembled and ordered.[10−12] Although LbL depositions onto nonflat colloidal particles or fibrillar textured structures have been investigated in previous studies, LbL depositions on nanostructured pores or patterns have recently been pursued.[13−20] In such cases, the chain conformation or complexation behavior of polyelectrolytes are completely different from those on flat surfaces due to the confinement effect arising from the nano/microstructures, which renders different growth characteristics in the LbL deposited films.

One notable aspect of the general LbL assembly method is that the order of layer stacking can be traced along the axial direction of the deposited film, generally from the bottom surface to the top surface.[21,22] It can provide a sequentially stacked multifunctionality to the film through incorporating specific material into the designated location within the multilayered films. In particular, this advantageous aspect has motivated the design of smart biomaterials as exemplified in drug-delivery materials.[23−25] However, due to the sequential deposition of each layer, there is an evident limitation in processing in terms of high-speed film growth. For example, since the unit size of stacking materials such as polyelectrolyte chains or nanoparticles is only on the order of nanometers to tens of nanometers, construction of a micrometer thick LbL film requires tedious repetition of the deposition process more

Received: January 13, 2012
Accepted: March 15, 2012
Published: March 22, 2012

than several hundred times. In an effort to overcome this limitation, instead of using a linearly growing system in which the film thickness is monotonically proportional to the LbL deposition number, alternative methods have been suggested, such as a use of exponentially growing polyelectrolyte pairs,[26−30] reinforcement of electrostatic interactions by an imposing external electric field,[31] or employment of a high-speed spraying LbL process.[32] On the basis of the understanding of this technical background, a novel and advanced means of LbL assembly is required wherein the structural characteristics and physical properties of the assembled films can be tailored in a precise and a rapid manner.

Here, we report a novel and robust means of depositing polyelectrolyte multilayers in three-dimensionally interconnected inverse opal (3D-IO) structures,[33−35] instead of conventionally used flat or simple two-dimensionally patterned substrates. Although LbL assembly within 3D-IO structures have been previously reported, the polyelectrolyte multilayers used therein have been mainly employed as thin adhesion promoting layers bound to charged biomolecules or inorganic precursors.[36,37] However, in this study, since the LbL assembly method allows for excellent processing controllability of a uniform film assembly even under the three-dimensionally confined environment, "effective high-speed deposition" with a considerable thickness can readily be realized; thus, functionalized thick films with several tens of micrometers in thickness can be constructed with repetitive LbL depositions less than several tens of times. In addition, mechanical properties of the assembled LbL films can be controlled through manipulating the skeletal frame of the inverse opal structures. These advantages offer easy fabrication of the structured films in the form of free-standing films, which is useful for various applications. As an exemplary demonstration for a practical use, we fabricate three-dimensionally structured porous nanofiltration membranes for separating multivalent metal ions, obtaining good separation efficiency while allowing for a high permeation flux of the medium. Considering its versatility for surface function modification under aqueous environments, this method can be utilized for applications in biomedical devices, microfluidic systems, and stimuli-responsive optical devices.

EXPERIMENTAL SECTION

Synthesis of Colloidal Nanoparticles. Ammonium persulfate (APS, reagent grade 98%) and polyvinylpyrrolidone (PVP, 55 000 M_w) were purchased from Aldrich. 2-Propanol (IPA, 99.5%), ethyl alcohol (EtOH, 99.9%), and styrene monomer (99.5%) were purchased from Samchun chemical, Korea. The monodispersed PS colloidal particles were prepared by a dispersion polymerization method.[38] In most experiments, a PVP stabilizer (0.01 g) was dissolved in 25 mL of ethanol or 2-propanol kept in a vial. A solution of APS initiator (0.0065 g) predissolved in 3 mL of deionized (DI) water was poured into the previously prepared solution. After stirring for several minutes, styrene monomer (2.2 mL) was added and the vial was put in a silicone oil bath maintained at constant temperature of 70−80 °C for 12 h. After completion of the polymerization reaction, the PS colloid solution was centrifuged at 15 000 relative centrifugal force (RCF) for 30 min and washed off with ethanol three times for removing the residual PVP.

Fabrication of Three-Dimensional Inverse Opal (3D-IO) Structures. Polyurethane acrylate (PUA, MINS-311RM, viscosity ~170 cps at 25 °C, Young's modulus after curing ~400 MPa) was purchased from Minuta technology, Korea.[39,40] The detailed procedure for fabricating free-standing three-dimensional inverse opal structures is illustrated in Figure 1. PS colloid particles were first dispersed in DI water (5 wt %). PS particles were then self-assembled into a three-dimensional ordered structure by evaporating a colloidal suspension at 60 °C on a glass substrate that was pretreated with plasma (PDC-001, Harrick Scientific Corp.) to generate hydrophilic surface groups. In order to fabricate the 3D-IO structures, UV-curable polyurethane acrylate (PUA) prepolymer was spin-coated onto the PS opal structure at 1000 rpm for 300 s. To remove the overcoated PUA from the top surface, an ethanol solution (30 v/v %) was repeatedly spin-coated at 1000 rpm for 60 s several times. To cure the void-filling PUA prepolymer under ambient atmospheric condition, UV-cuing with at least 3 h was applied since the oxygen molecules in air worked as radical scavenger of the UV-curing reaction.[39] After the UV-curing process, the sample was immersed in toluene (good solvent for PS) for 2 h to remove the PS colloidal particles. The resulting inverse PUA opal structure was easily peeled off from the substrate, resulting in a free-standing phase of 3D-IO structures.

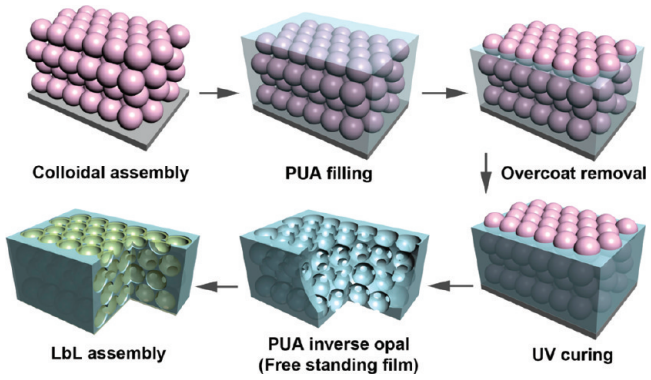

Figure 1. Schematic procedure of fabricating free-standing three-dimensional inverse opal (3D-IO) structure followed by layer-by-layer deposition of polyelectrolyte multilayers inside 3D-IO templates.

Layer-by-Layer (LbL) Deposition of Polyelectrolyte Multilayers Inside 3D-IO Templates. Poly(allylamine hydrochloride) (PAH, 15 000 M_w) and poly(sodium 4-styrenesulfonate) (PSS, 70 000 M_w) were purchased from Aldrich. All chemicals were used as-received. PAH and PSS were prepared as 20 mM solutions in mixed water/2-propanol solvent (80:20 v/v), respectively, on the basis of the repeat-unit molecular weight. The pHs of the PAH and PSS solutions were carefully adjusted with dilute solutions of hydrochloric acid and sodium hydroxide. Layer-by-layer deposition was performed using either a programmable slide stainer (HMS70, Microm) or manually under the deposition conditions of adsorption of polyelectrolyte for 8 min followed by three sequential washing steps (1 min for each) in a DI water bath.

Membrane Test of LbL Assembled 3D-IO Structures. Measurements of the membrane performance in an ion separation application were carried out using a stirred cell module (Amicon 8010, Millipore Corp.) with a pressurized vessel at room temperature. The stirred cell (stirred at 400 rpm) had an effective membrane area of 4.1 cm^2. The system was pressurized with N_2 to 4.8 bar, and the feed vessel was filled with a 600 mL solution of 20, 100, or 1000 ppm $CuSO_4$. Both sides of the IO membrane were covered with cellulose acetate membranes (pore size 0.45 μm, Whatman Corp.) as a supporting material. After stabilizing the membrane system for 6 h, a certain amount of permeated samples were then collected.

Characterization of LbL-Assembled Films. The changes in film thickness of the assembled polyelectrolyte multilayers with varying assembling pH value were measured by ellipsometry (SEMF-1000, Nanoview, Korea). The surface morphology of the assembled polyelectrolyte multilayers was observed with an atomic force microscope (AFM, Dimension 3100, Veeco). Changes in the surface morphology of the assembled polyelectrolyte multilayer inside the inverse opal structure in response to the variation of assembling pH were observed with a scanning electron microscope (SEM, JSM-7401F, JEOL). In the course of the membrane test, atomic absorption

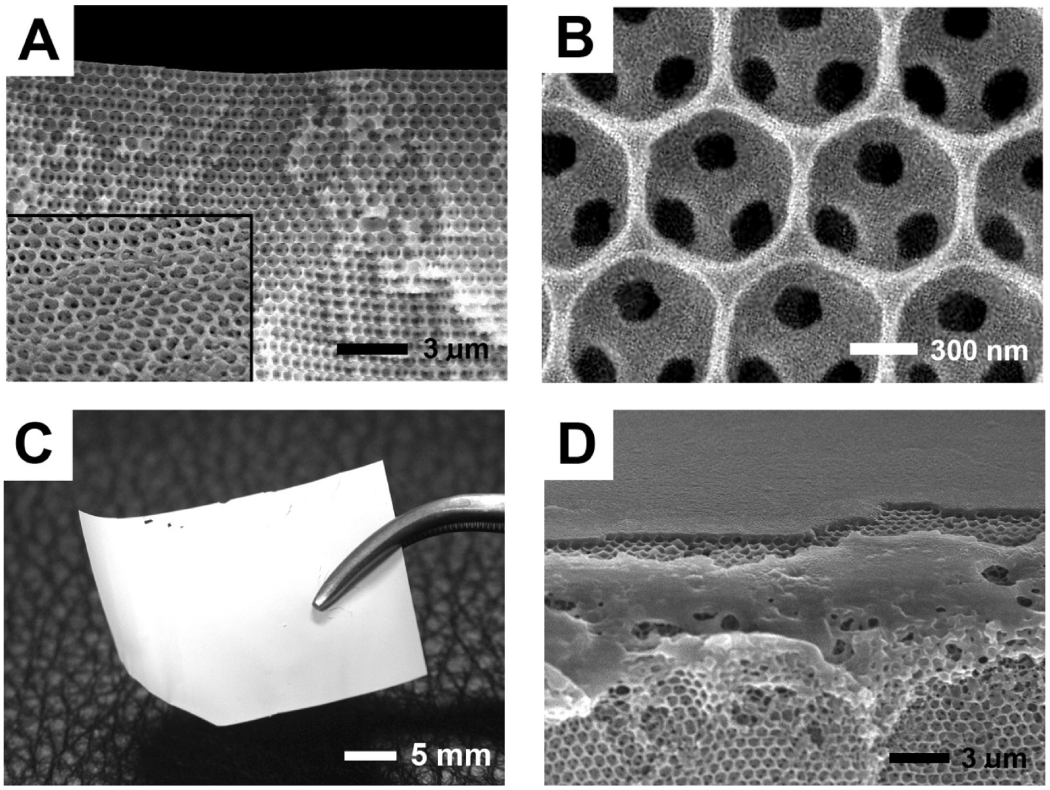

Figure 2. (A) Cross-sectional scanning electron microscopic (SEM) image of well-ordered 3D-IO structure of PUA. The inset reveals the complete opening of pores on the top surface. (B) SEM observation for top surface of 3D-IO PUA structure. (C) Magnified photograph of flexible free-standing 3D-IO films demonstrated with a large scale (sample size is 2 cm × 2.8 cm). (D) SEM image of the surface of the 3D-IO structure treated with LbL depositions under fully aqueous conditions. Due to the strong hydrophobicity of PUA frame, polyelectrolyte chains are agglomerated on the top surface and do not penetrate inside 3D-IO structures.

spectroscopy (AAS, Buck 210VGP) was used to accurately determine the cation concentration of the permeated solution.

RESULTS AND DISCUSSION

Figure 1 shows a schematic procedure of fabricating the three-dimensional inverse opal (3D-IO) structure and its subsequent surface modification with a LbL assembly of polyelectrolyte multilayers. First, PS colloidal particles are self-assembled to an ordered opal structure, and the voids between particles are filled with a UV-curable prepolymer of PUA. After curing the PUA with UV irradiation, PS colloidal particles are removed by an organic solvent of toluene, leading to the formation of an inverse-opal structured PUA frame. For a LbL assembly within a 3D-IO template, the structured PUA layer is peeled off from the substrate and forms a free-standing film. Finally, through applying LbL assembly for the polyelectrolyte multilayers, three-dimensionally structured functional polyelectrolyte films can be constructed.

In order to form colloidal opal structures, several methods can be employed, including sedimentation,[41] shear flow,[42] spin coating,[43] or evaporative deposition.[44−46] Since our approach is targeted to form large-scale free-standing films of 3D-IO structures, the evaporative deposition method is the most plausible. Therein, the ordered colloidal phase can be readily constructed with controllable thickness and size by the competitive control between assembling rate and settling rate of colloidal particles via adjusting the evaporation temperature.[45] When the temperature is too low, the settling rate is faster than the rate of particle ordering at the solution surface, thereby causing an irregularity in the colloidal ordering. In contrast, upon applying a high temperature, the rate of surface ordering of colloidal particles conversely exceeds the settling rate due to an enhanced evaporation of dispersing medium. However, since the evaporation-induced ordering is localized at different locations on the sample surface, uniform control over the film thickness is difficult to achieve under such a condition. Therefore, in this study, a temperature of 60 °C was chosen as the optimum for creating the well-ordered and large-scale-demonstrated opal structures of colloidal particles.

Next, some important issues for fabricating 3D-IO structures are to be considered. The first required property is the physical and mechanical stability of the frame material. Although lots of research has been performed focusing on 3D-IO structure fabrication with various materials, typically, for the case of using inorganic precursors,[35,47,48] the solidified structure is mechanically brittle and prone to collapse and cleavage due to an excessive rate of volumetric shrinkage upon solidification. This disadvantageous aspect generally makes 3D-IO structures impractical for large-scale realization in the form of free-standing films. Therefore, in order to overcome this drawback, we employ the polymeric prepolymer of PUA as a frame material of which volumetric shrinkage rate upon cross-linking is less than 3%, which ensures the structural interconnectivity over a large scale even after UV curing.[39,40] In addition, due to its outstanding chemical inertness, it can eliminate concerns of structural deformation and chemical degradation during postprocessing, e.g., colloidal removal with organic solvent or LbL assembly in aqueous condition.

The second prerequisite for an appropriate 3D-IO frame material is excellence in fabricating the free-standing films with

double-sided open porosity. In terms of 3D-IO structures constructed on a supporting substrate, the bottom layer spontaneously provides surface porosity since the colloidal template makes contact with the substrate; hence, the PUA prepolymer cannot penetrate the interface between the colloidal particles and the substrate. On the other hand, the surface porosity for the top layer on the opposite side is not readily attainable. In principle, if the prepolymer can be partially filled inside the opal-structured template, i.e., by applying a thinner coating than the thickness of the colloidal opal structures, the top surface can have open porosity. However, for the case of actual processing, a fairly viscous prepolymer slowly permeates into the opal-structured template and completely covers the colloidal surface due to a strong wetting characteristic of PUA prepolymer, which leads to the formation of a problematic overcoat on the surface. As a result, it is generally observed that only the bottom side has an open porosity, whereas the top surface is blocked by the overcoated layer of PUA. In order to achieve a double-sided open porosity, the overcoated excess of PUA prepolymer is selectively removed by a spin-coating process with ethanol which is a noncompatible solvent with the PUA prepolymer. Since the PUA overcoat is physically removed by the shear-slip action of ethanol during spin-coating, optimal adjustment of the viscosity of the PUA prepolymer is imperative for attaining open porosity. While the highly viscous PUA prepolymer involves much longer chain conformation, thus enhancing the structural flexibility of 3D-IO structures after curing, its stronger cohesion makes permeation into the opal-structured template poor and reduces the effectiveness of removing the overcoated layer, eventually yielding an incomplete PUA filling or unsuccessful surface opening. Therefore, control of the viscosity for the PUA prepolymer is needed as well. Figure 2A shows successfully fabricated 3D-IO structures of UV-cross-linked PUA, wherein the top surface is completely opened with pores and the cross-sectional observation reveals the perfectly ordered structures of the 3D-IO PUA frame. A detailed observation for the 3D-IO structure presented in Figure 2B reveals that individual voids inside the structures are interconnected with pores of 180−200 nm in diameter. Also, a magnified photograph shown in Figure 2C shows that the 3D-IO PUA structure can be fabricated as flexible free-standing films with little defect over a large scale.

Prepared free-standing films of 3D-IO PUA structures can be utilized for further functionalization with a LbL multilayer deposition method. Most of the polyelectrolyte chains are ionized under an aqueous environment so as to create strong electrostatic attraction between oppositely charged groups.[21,22] A possible concern encountered in this system for the LbL assembly of polyelectrolyte multilayers is the strong hydrophobic nature of 3D-IO PUA templates.[39] While the internal structures of 3D-IO PUA frame, which are created from the self-assembly of PS colloidal particles of 800 nm in diameter resulting in interconnected pores 180−200 nm in diameter, are expected to exhibit strong capillary action due to the small pore size, the intrinsic hydrophobicity of PUA (water contact angle = 135 degrees) suppresses the spontaneous wetting of aqueous polyelectrolyte solutions inside the 3D-IO PUA template. Therefore, polyelectrolyte chains are locally adsorbed on the very top surface of the 3D-IO structures by hydrophobic interactions and self-agglomeration (Figure 2D). To overcome this drawback of the localized deposition of polyelectrolyte multilayers on the nanostructured porous surfaces, previous studies have adopted a means of imposing external pressure[15,20] to induce the internal flow inside the porous channel in such a way that even the hydrophobic structures could be amenable to LbL deposition. However, this approach is strongly limited for a large-scale and continuous processing.

Meanwhile, surface modification of flat surfaces can be achieved with simple plasma treatment. This enables a transition of the surface characteristic from hydrophobic to hydrophilic; e.g., even a Teflon coated surface can be exploited for aqueous LbL deposition after a short-period plasma treatment without affecting the uniformity and stability of the deposited films.[49] However, for the case of the 3D-IO PUA template having a thickness on the order of several tens of micrometers, the plasma treatment is inadequate for modifying the entire region inside the 3D-IO structures. Rather, a longer period of plasma treatment can accelerate the dissociation of carbon chains of PUA, which in turn, induces the structural collapse of the surface region. To address these challenges, we utilize an alcohol-mixed solvent as a medium for the polyelectrolyte solutions. If DI water is mixed with 2-propanol (20 vol %), the wetting of the 3D-IO PUA template can be greatly enhanced by the lower surface tension of the alcohol, thereby yielding a significant decrease in the contact angle from 135° to 80°.[50,51] Although facilitated wetting is expected for a higher content of 2-propanol, the dielectric characteristics of the aqueous mixture adversely decreases, which may reduce the charged characteristic of polyelectrolyte chains. Therefore, to obtain electrostatic interactions for LbL assembly without sacrificing the wetting properties, an appropriately adjusted mixing ratio of 2-propanol is required.

As has been reported in previous work, polyelectrolyte multilayer films show different behavior in terms of film growth and surface morphology according to the variation of the charged condition of polyelectrolyte chains.[21,52] Influential factors are known to be the type of polyelectrolytes,[19] salt concentration,[22,53] or pH condition[54,55] of LbL deposition. In order to investigate the film deposition characteristics in 3D-IO structured templates, we used cationic poly(allylamine hydrochloride) (PAH) and anionic poly(sodium 4-styrenesulfonate) (PSS) as a pair for LbL assembly (hereafter denoted as PAH/PSS). This polyelectrolyte pair offers an advantage in that the pH variation of the LbL assembly condition can be visualized through different morphologies of the deposited film inside 3D-IO structures. Although other representative weakly charged polyelectrolyte pairs can be used as well, such as PAH and poly(acrylic acid) (PAA), which is known to show a marked response to the pH variation during film deposition,[9,54,55] the PAH/PSS pair is chosen to be more appropriate in this study considering its potential applicability for nanofiltration membranes. Since the ionic complexation in the PAH/PAA pair is known to be much denser than that in PAH/PSS,[56,57] the permeation flux of the membrane with the PAH/PAA pair is expected to be relatively low even under the identical performance in the ion rejection rate.

In terms of the PAH/PSS pair, although their acid dissociation constants (pK_a) in DI water are 8.8 and 1.0, respectively, pK_a values shift to the neutral range to some extent under the mixed solvent condition since the dielectric environment is substantially weakened.[58] As a result, the charge density of the polyelectrolyte chains decreases and the degree of chain entanglement conversely increases. Indeed, the pK_a of PAH (intrinsic base) decreases, whereas that of PSS (intrinsic acid) increases.[59−61] On the basis of the understanding of this tendency of pK_a shift in the mixed solvent

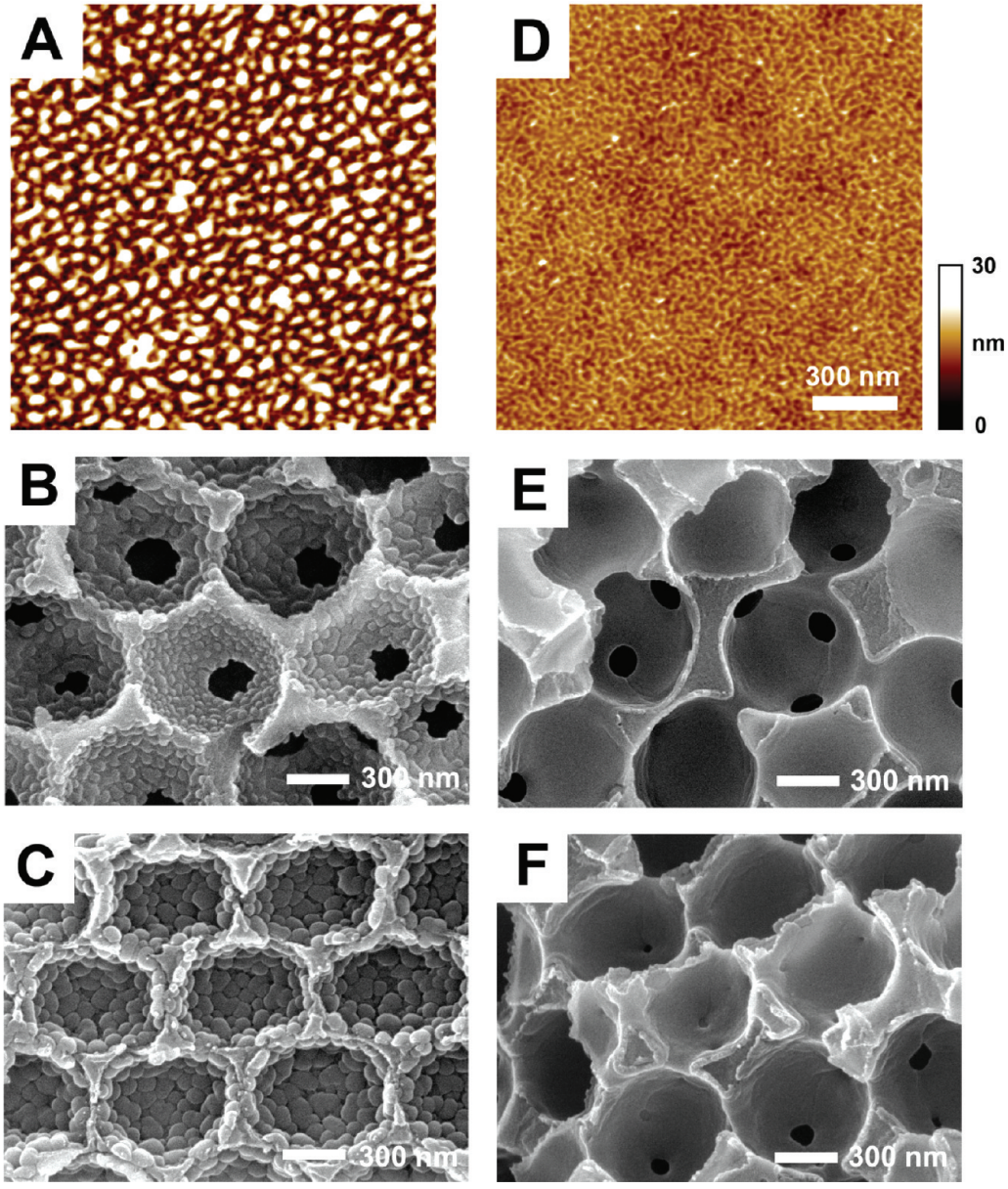

Figure 3. Comparison of the growth behavior of LbL deposited films inside 3D-IO structures according to the assembly pH conditions. (A, B, C) AFM and SEM observations for PAH/PSS depositions under highly entangled chain conditions. 2.5 bilayer sets on flat PUA surface (A), 5.5 bilayer sets for (B), and 27.5 bilayer sets for (C) assembled within 3D-IO PUA at pH 9.3/9.3 and 2.3/2.1, respectively. (D, E, F) AFM and SEM observations for PAH/PSS depositions under strongly stretched chain conditions. 5.5 bilayer sets on flat PUA surface (D), 30.5 bilayers sets for (E), and 35.5 bilayer sets for (F) assembled within 3D-IO PUA at a pH of 4.5/4.5. For AFM images in (A) and (D), the scanned area is 1.5 μm × 1.5 μm and z-scale is 30 nm.

system, the pH of the LbL deposition was varied for two contrasting regimes: one for highly entangled polyelectrolyte chains and the other for highly stretched chains. When the pH conditions of 9.3/9.3 or 2.3/2.1 are applied for LbL assembly of PAH/PSS, strong chain entanglement can take place for PAH in the former and for PSS in the latter, respectively.[62] Since a lower charge density is maintained for polyelectrolyte chains due to the shift of the pK_a value, chain entanglement is intensified and the free volume inside the polymeric chains increases as well. Moreover, it is also expected to show hydrophobic adsorption of less charged polyelectrolyte chains on the neutral hydrophobic surface of PUA, yielding globular shapes in the deposited film.[63] Consequently, one can expect concurrent increases in the film growth rate and the surface roughness. In order to ensure the influence of hydrophobic adsorption, we observe the structures of surface-deposited PAH/PSS films assembled at pH conditions of 9.3/9.3 or 2.3/2.1 on flat a PUA surface. As a result, 2.5 bilayer depositions of PAH/PSS create a prominent island-like morphology on the surface (Figure 3A), which is indicative of a partial wetting of slightly charged polyelectrolyte chains on neutral surface. A similar tendency is retained in the internal space of 3D-IO PUA templates as shown in Figure 3B,C, in which a raspberry-like film deposition is manifest, indicative of hydrophobic adsorptions as well as stronger chain entanglements. As the number of the film deposition cycles increases, the domain size of the ionic complexation also increases, whereas the pore size of the interconnection decreases.

On the other hand, a pH condition of 4.5/4.5 is used for suppressing chain entanglement, under which the polyelectrolyte chains of PAH and PSS are both strongly charged and highly stretched. Therefore, the adsorbed chains form flat deposited films with reduced surface roughness. This tendency is also verified from the experiments on flat PUA surface, in which a complete coverage of PAH/PSS films with a minimal surface roughness is observed (Figure 3D). Further, the rate of film growth is significantly retarded, as compared to the case of highly entangled polyelectrolyte chains. As can be verified in Figure 3E,F, monotonous film deposition due to an adsorption of the stretched chains is typically observed inside the 3D-IO PUA templates. Although the surface texture of the deposited films is fairly smooth and the deposition rate is thus reduced compared to the cases of entangled polyelectrolyte chains, an increase in the deposited film thickness accounts for continuous film growth in 3D-IO structures with increasing the number of bilayers. One notable aspect observed in LbL deposited 3D-IO templates is the uniformity of the deposited films throughout the porous structure, manifesting the robustness and effectiveness of this process. This, notwithstanding, deposition of the internal film becomes limited as the pores of the interconnected channels become narrower with increasing LbL deposition number. Therefore, after final stage of LbL coating inside the 3D-IO structure, void regions still remain in the center of each pore. In order to estimate the volume fraction of residual voids, we sequentially measured the mass increment of the 3D-IO structured sheet (2.5 cm × 7.5 cm × 30 μm); initial mass of 0.015 g of 3D-IO PUA frame was increased to 0.029 g (fully dried condition) after complete LbL assembly of PAH/PSS at pH 2.3/2.1 (as shown in Figure 3C). This result corresponds to the volumetric composition of 24.3% of PUA, 20.7% of PAH/PSS complexes, and 55.0% of void.

LbL film growth behavior in 3D-IO structures is sequentially monitored and plotted in Figure 4. Simultaneously, the influence of surface hydrophobicity on the growth behavior of LbL deposited films is investigated by employing different substrates of hydrophilic Si and hydrophobic PUA (flat PUA surface cured on Si wafer).[63] For the case of the PAH/PSS pair deposition on a flat substrate under aqueous solvent conditions in the absence of salt dissolution, strong ionic complexation takes place and a linearly growing characteristic is observed as shown in Figure 4A.[21] However, since the dielectric constant decreases for the mixed solvent condition, the degree of dissociation of polyelectrolyte chains (charge density) is decreased as well, and chain entanglement is reinforced, resulting in accelerated film growth even on a flat substrate,[52,64] as shown in Figure 4B. This result is analogous to the film growth in aqueous LbL deposition with salt dissolution, in which the charge screening effect induces entanglement of the polyelectrolyte chains and the increased surface roughness. Also, this transition in growth regime from a linear to exponential system potentially suggests the occurrence of interdiffusion of polyelectrolyte chains within a weakly bound structure of the PAH/PSS. Since the weaker electrostatic interactions under mixed solvent condition can allow for free migration of polyelectrolyte chains within the ionically complexed multilayers, the assembled film can act as a reservoir of free polyelectrolyte chains, eventually leading to an exponential film growth with increasing the deposition numbers.[26,27,29] This characteristic needs to be further investigated, such as with fluorescence study. In terms of the surface hydrophobicity, the film growth behaviors are similar

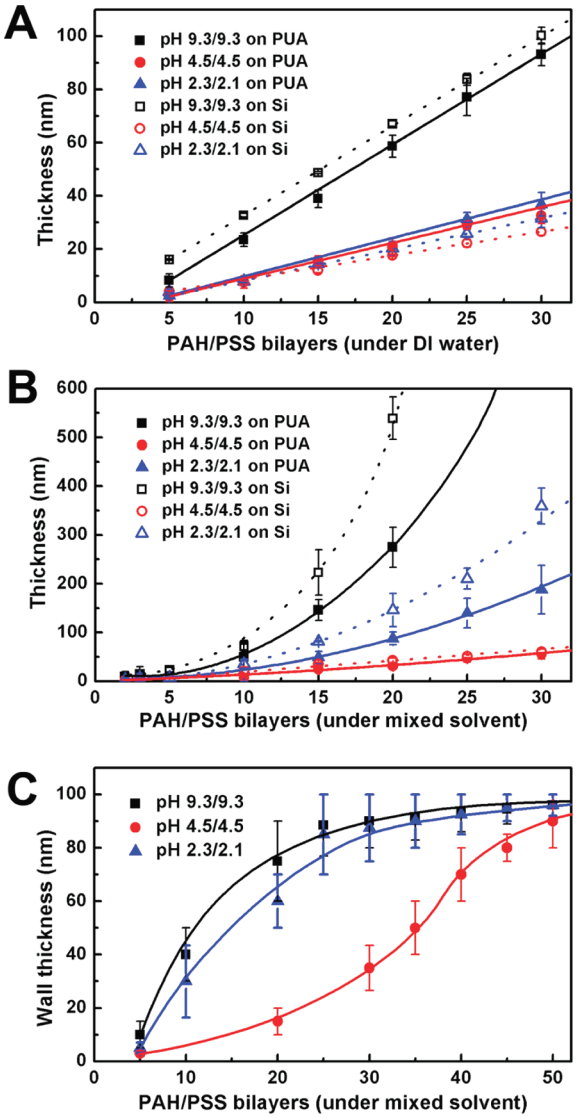

Figure 4. Film growth behavior of PAH/PSS multilayers under different environments with varying pH, types of solvent, surface hydrophobicity, and structural conditions of substrate. The stepwise increase in the thickness is measured and monitored by ellipsometric (for flat surfaces) and SEM observations (for 3D-IO structures). (A) Linearly growing behavior on a flat surface using DI water solvent without adding salts. (B) Nonlinearly or exponentially growing behavior on a flat surface using a mixed water/2-propanol solvent (80:20 v/v). Under identical pH conditions of LbL deposition, the film growth rates are observed to be relatively faster on the hydrophilic Si than those on the hydrophobic PUA surface. (C) Saturated film growth behavior inside 3D-IO structures using the mixed solvent. Error bars indicate the standard deviation.

irrespective of the substrate type. However, the film growth rate is relatively retarded for the case of hydrophobic PUA substrates, on which the partial wetting and nucleation of adsorbed polyelectrolyte chains in the earlier stage of LbL deposition impede the rate of LbL film assembly.

In contrast, the LbL deposition of PAH/PSS under mixed solvent conditions is observed to be significantly retarded in the 3D-IO structures as shown in Figure 4C, wherein the film growth rate is slow with an order of magnitude compared to that on the flat substrates. This result is contrasted to previous studies reporting an accelerated rate of film growth on

patterned or nanostructured surfaces.[13,15,19] For the case of two-dimensional nanopatterns on the substrate, polyelectrolyte diffusion and subsequent surface adsorption is facilitated due to the direct contact of polyelectrolyte solution above the patterns while minimizing the desorption of polyelectrolytes during washing due to strongly confined conditions within nanopatterns. As a result, an accelerated film growth characteristic is expected. However, when the patterns are three-dimensionally structured, including numerous porous channels several hundred nanometers in diameter over a range of tens of micrometers in thickness, the diffusion of polyelectrolyte chains stagnates and the replenishment from the outer solution is greatly limited after the polyelectrolyte solution infiltrates the 3D-IO structures, leading to a reduced rate in the LbL deposition; this leads to a reduced LbL deposition rate.

Along with the suppressed diffusion of polyelectrolyte chains, the low deposition rate can be attributed to the reinforced electrostatic repulsion between closely neighbored same kind of charges within three-dimensionally confined nanostructures.[13] Unlike two-dimensional planar structures on which the electrostatic interactions directionally work along the axial direction of film deposition, the electrostatic interactions inside three-dimensional nanostructures take place isotropically, wherein the additional binding of the polyelectrolyte chains are self-regulated due to the increased repulsive interactions. Therefore, the film growth rate is slow and eventually ceased after the saturation of polyelectrolyte adsorption.[17,18,20] After the saturation point, the internal pores within 3D-IO structures are plugged by the LbL deposited films. When the polyelectrolyte chains are highly entangled, such as at pH conditions of 9.3/9.3 or 2.3/2.1, the internal pores of the 3D-IO structures completely disappear after 25−30 bilayer depositions. On the other hand, upon applying the highly stretched chain condition at pH 4.5/4.5, the saturation point is observed after 45−50 bilayer depositions. However, it should be noted in this regard that several tens of micrometers-thick 3D-IO structures can be uniformly coated by LbL deposition with only several tens of repetitions, which is orders of magnitude faster than conventional LbL processing on flat surfaces. Therefore, the effective high-speed LbL deposition of functional moieties can be readily achievable with this method.

In order to demonstrate the feasibility of 3D-IO structures for practical applications, we tested them as nanofiltration (NF) membranes.[65,66] LbL film-based NF membranes have been extensively investigated by previous studies,[56,67−69] in which the LbL assembled films having a skin layer around 50 nm in thickness are usually placed on the supporting nanoporous membranes made of polyethersulfone (PES) or anodic aluminum oxide (AAO). In particular, LbL assembled films are beneficial for enhanced NF membrane performance since the charged polyelectrolyte chains can induce efficient Donnan exclusion and create the steric exclusion effect via control over internal free volume of the ionically complexed films.[70,71] Therefore, if the 3D-IO structures can be appropriately utilized for NF membranes, maximized Donnan exclusion against ionic transport can be expected since they include numerous interfaces of polyelectrolyte multilayers within three-dimensionally interconnected pores. In addition, shell-like films deposited inside the respective IO domains undergo volumetric expansion with swelling during the solution permeation process. However, due to the presence of an internal PUA frame, swelling-induced pressure or deformation rarely affects the mechanical rigidity and stability of the 3D-IO membranes, minimizing the destructive erosion of the LbL films by salt permeation or excessive flow of the feed solution.

Various types of polyelectrolyte pairs can be exploited for removal of multivalent cations for water treatment.[72] As mentioned previously, in this study, we have chosen PAH/PSS since this pair can provide a high rejection rate of multivalent cations while maintaining a relatively good level of permeation flux. In terms of PAH, in particular, the branched ammonium groups ($-CH_2NH_3^+$) offer a high flexibility to the chains, thus exhibiting highly efficient removal of multivalent cations. To facilitate this property, a lower range of pH should be applied during LbL deposition. Otherwise, cationic PAH is readily deprotonated and the charge density decreases, which results in an increased incorporation of the nonionized chain segments.[67] Consequently, the excess charge concentration is reduced; hence, the removal efficiency of cations decreases. Therefore, an acidic LbL deposition condition at pH 2.3/2.1 was employed for NF membranes experiments. In addition, as was verified in Figure 4, nonsalt dissolved and solvent-mixed (DI water:IPA = 80:20 v/v) polyelectrolyte solutions were used to suppress the preferential polyelectrolyte adsorptions on the surface and to obtain a uniform conformal coating inside the 3D-IO structures.

The 3D-IO PUA templates are LbL deposited repeatedly more than 25 times with a PAH/PSS complexed pair so as to block the internal pores of 3D-IO structures. An additional 4−5 depositions of $(PAH/PSS)_nPAH$ bilayers form a ∼50 nm-thick surface coating layer, which ensures the complete passivation of 3D-IO structures with LbL assembled films. Also, to significantly improve the Donnan exclusion effect for cationic ions, the top layer of the PAH/PSS membrane is treated with PAH, which is positively charged.[68] The prepared 3D-IO NF membranes were then attached to cellulose acetate (CA) supporting membranes on both sides for easy installation inside the membrane testing system (Amicon cell). It should be noted that the CA supporting membranes used here rarely affect the membrane performance since the pore size of the CA membranes is much larger than that of 3D-IO structures. Further, nanoporous PES or AAO supporting membranes were not chosen here as they strongly affect the permeation flux of the separation process due to their very small internal pore sizes.

For the membrane tests of metal ion separation, a copper sulfate solution (20 ppm concentration) was applied as a feed solution and the permeate concentration was measured by atomic absorption spectroscopy (AAS). After equilibrating the membrane cell for 6 h, the rejection rate of the copper(II) ions was measured to be 94.9%, which is excellent performance under highly diluted feed conditions. In order to ensure the main role of the branched ammonium groups for efficient removal of cations, the 3D-IO membranes assembled at higher pH conditions (4.5/4.5 and 9.3/9.3) were also prepared and tested for copper ions rejection. The resulting rejection rates were measured as 72.2% and 62.0%, respectively, which proved the importance of acquiring the stabilized Donnan exclusion condition. We also observed the inner structures of 3D-IO membrane after the filtration test if there has been structural collapse or deformation due possibly to the applied pressure and polyelectrolyte swelling. However, there has been no noticeable change in the internal structure as compared to the cases presented in Figure 3. As shown in Table 1, the separation performance of the 3D-IO membranes exhibits a change in response to the variation of feed concentrations. When copper

Table 1. Solution Fluxes and Cu^{2+} Rejections with PAH/PSS Films Deposited at pH 2.3/2.1 Inside 3D-IO Structured Membrane

concentration of Cu^{2+} (ppm)	rejection of cations (%)	flux (m^3 m^{-2} day^{-1})
20	94.9 ± 2.6	30 ± 1
100	95.4 ± 2	32 ± 0.5
1000	81.7 ± 3	32 ± 0.5

sulfate solutions of 100 or 1000 ppm in concentration were used, the rejection rate of the copper(II) ions was determined to be 95.4% and 81.7%, respectively. The reason for the slight decrease in the rejection rate for the high concentration condition can be ascribed to the concentration polarization that is associated with the shielding effect caused by the increased ion concentrations near the membrane surface.[73] If the thickness of the outermost surface layer is further increased with additional bilayer depositions, a more enhanced rejection rate can be expected, whereas the resistance to permeation will increase.[67]

More notably, the permeation flux is measured as 30 m^3/m^2·day, which is an order of magnitude larger than that from conventional LbL coated membranes (usually observed in the range of 1−4 m^3/m^2·day under an applied pressure of 4.8 bar).[68,72,74,75] This can be primarily attributed to the structural characteristics of the 3D-IO membranes. In general, PES membranes or track-etched membranes have a smaller areal density of surface pores, which results in a relatively low permeation flux against the applied pressure. On the other hand, for the case of 3D-IO membranes, the PUA frame is highly porous and the pores are completely developed over the surface. In addition, the inner deposited LbL films are water-swellable and readily allow for aqueous permeation, yielding an enhanced permeation flux without sacrificing ion rejection capability. Although the enhanced permeation flux is expected to be obtained with applying greater pressure (e.g., over 30 bar, much as used in the modern membrane industry), this study deals with a proof-of-concept of 3D-IO membranes under conventional operation pressure for NF membranes.

CONCLUSIONS

In summary, we fabricated 3D-IO structures of UV-curable PUA polymer using a colloidal opal phase as a structuring template and then subsequently applied LbL deposition of polyelectrolyte multilayers inside the 3D-IO structures. As a result, different film deposition behaviors were observed as compared to use of conventional flat or two-dimensionally patterned substrates. Although the 3D-IO structured PUA frame is intrinsically strongly hydrophobic, uniformly deposited films can be grown even inside the 3D-IO structures. This is because films are free-standing with a double-sided open porosity, and the surface wettability can be tuned when deposition takes place in a mixed solvent condition of water/alcohol. In addition, through the control over polymeric chain entanglement using pH variation for LbL deposition, different morphologies of the LbL assembly were obtained. From a structural viewpoint, water-swellable and permeable polyelectrolyte multilayer films form independent shell structures inside the submicrometer-sized single domain of the 3D-IO structures. However, since these unit structures are interconnected and confined within the chemically inert and mechanically stable IO frame of PUA, they are potentially useful as nanofiltration membranes. After applying the PAH/PSS pair-deposited 3D-IO films as nanofiltration membranes for removal of diluted copper ions, we obtained excellent membrane performance simultaneously exhibiting a good rejection rate and a high permeable flux. Therefore, if further tailored and controlled, it is anticipated that these materials can be utilized for large scale fabrication of next generation nanofiltration membranes.

AUTHOR INFORMATION

Corresponding Author

*E-mail: pjyoo@skku.edu.

Notes

The authors declare no competing financial interest.

ACKNOWLEDGMENTS

This work was supported by Basic Science Research Program grants (2010-0027771, 2010-0029409) and a research grant (NRF-C1AAA001-2010-0028962) through the National Research Foundation of Korea (NRF) funded by the Korea Government (MEST). This research was also supported by a grant (10037872) from the Fundamental R&D Program for Technology of World Premier Materials funded by the Ministry of Knowledge Economy (MKE) of Korea.

REFERENCES

(1) Decher, G. *Science* **1997**, *277*, 1232−1237.
(2) Hammond, P. T. *Adv. Mater.* **2004**, *16*, 1271−1293.
(3) Hiller, J.; Mendelsohn, J. D.; Rubner, M. F. *Nat. Mater.* **2002**, *1*, 59−63.
(4) Lee, D.; Rubner, M. F.; Cohen, R. E. *Nano Lett.* **2006**, *6*, 2305−2312.
(5) Shimomura, H.; Gemici, Z.; Cohen, R. E.; Rubner, M. F. *ACS Appl. Mater. Interfaces* **2010**, *2*, 813−820.
(6) Wood, K. C.; Zacharia, N. S.; Schmidt, D. J.; Wrightman, S. N.; Andaya, B. J.; Hammond, P. T. *Proc. Natl. Acad. Sci. U.S.A.* **2008**, *105*, 2280−2285.
(7) Lee, S. W.; Kim, B. S.; Chen, S.; Shao-Horn, Y.; Hammond, P. T. *J. Am. Chem. Soc.* **2009**, *131*, 671−679.
(8) Lee, J. S.; Cho, J.; Lee, C.; Kim, I.; Park, J.; Kim, Y. M.; Shin, H.; Lee, J.; Caruso, F. *Nat. Nanotechnol.* **2007**, *2*, 790−795.
(9) Mendelsohn, J. D.; Barrett, C. J.; Chan, V. V.; Pal, A. J.; Mayes, A. M.; Rubner, M. F. *Langmuir* **2000**, *16*, 5017−5023.
(10) Zheng, H. P.; Lee, I.; Rubner, M. F.; Hammond, P. T. *Adv. Mater.* **2002**, *14*, 569−572.
(11) Toca-Herrera, J. L.; Krastev, R.; Bosio, V.; Kupcu, S.; Pum, D.; Fery, A.; Sara, M.; Sleytr, U. B. *Small* **2005**, *1*, 339−348.
(12) Yoo, P. J.; Nam, K. T.; Belcher, A. M.; Hammond, P. T. *Nano Lett.* **2008**, *8*, 1081−1089.
(13) Lee, D.; Nolte, A. J.; Kunz, A. L.; Rubner, M. F.; Cohen, R. E. *J. Am. Chem. Soc.* **2006**, *128*, 8521−8529.
(14) Pallandre, A.; Moussa, A.; Nysten, B.; Jonas, A. M. *Adv. Mater.* **2006**, *18*, 481−486.
(15) Alem, H.; Blondeau, F.; Glinel, K.; Demoustier-Champagne, S.; Jonas, A. M. *Macromolecules* **2007**, *40*, 3366−3372.
(16) DeRocher, J. P.; Mao, P.; Han, J. Y.; Rubner, M. F.; Cohen, R. E. *Macromolecules* **2010**, *43*, 2430−2437.
(17) Lazzara, T. D.; Lau, K. H. A.; Abou-Kandil, A. I.; Caminade, A. M.; Majoral, J. P.; Knoll, W. *ACS Nano* **2010**, *4*, 3909−3920.
(18) Kim, J. Y.; DeRocher, J. P.; Mao, P.; Han, J.; Cohen, R. E.; Rubner, M. F. *Chem. Mater.* **2010**, *22*, 6409−6415.
(19) Kim, Y. H.; Lee, Y. M.; Park, J.; Ko, M. J.; Park, J. H.; Jung, W.; Yoo, P. J. *Langmuir* **2010**, *26*, 17756−17763.
(20) Azzaroni, O.; Lau, K. H. A. *Soft Matter* **2011**, *7*, 8709−8724.
(21) Schlenoff, J. B.; Ly, H.; Li, M. *J. Am. Chem. Soc.* **1998**, *120*, 7626−7634.
(22) Schlenoff, J. B.; Dubas, S. T. *Macromolecules* **2001**, *34*, 592−598.

(23) Tang, Z. Y.; Wang, Y.; Podsiadlo, P.; Kotov, N. A. *Adv. Mater.* **2006**, *18*, 3203−3224.
(24) Zacharia, N. S.; Modestino, M.; Hammond, P. T. *Macromolecules* **2007**, *40*, 9523−9528.
(25) Katagiri, K.; Nakamura, M.; Koumoto, K. *ACS Appl. Mater. Interfaces* **2010**, *2*, 768−773.
(26) Picart, C.; Mutterer, J.; Richert, L.; Luo, Y.; Prestwich, G. D.; Schaaf, P.; Voegel, J.-C.; Lavalle, P. *Proc. Natl. Acad. Sci. U.S.A.* **2002**, *99*, 12531−12535.
(27) Lavalle, P.; Gergely, C.; Cuisinier, F. J. G.; Decher, G.; Schaaf, P.; Voegel, J.-C.; Picart, C. *Macromolecules* **2002**, *35*, 4458−4465.
(28) Yoo, P. J.; Nam, K. T.; Qi, J. F.; Lee, S. K.; Park, J.; Belcher, A. M.; Hammond, P. T. *Nat. Mater.* **2006**, *5*, 234−240.
(29) Zacharia, N. S.; DeLongchamp, D. M.; Modestino, M.; Hammond, P. T. *Macromolecules* **2007**, *40*, 1598−1603.
(30) Yoo, P. J.; Zacharia, N. S.; Doh, J.; Nam, K. T.; Belcher, A. M.; Hammond, P. T. *ACS Nano* **2008**, *2*, 561−571.
(31) Ko, Y. H.; Kim, Y. H.; Park, J.; Nam, K. T.; Park, J. H.; Yoo, P. J. *Macromolecules* **2011**, *44*, 2866−2872.
(32) Krogman, K. C.; Lowery, J. L.; Zacharia, N. S.; Rutledge, G. C.; Hammond, P. T. *Nat. Mater.* **2009**, *8*, 512−518.
(33) Zakhidov, A. A.; Baughman, R. H.; Iqbal, Z.; Cui, C. X.; Khayrullin, I.; Dantas, S. O.; Marti, I.; Ralchenko, V. G. *Science* **1998**, *282*, 897−901.
(34) Blanco, A.; Chomski, E.; Grabtchak, S.; Ibisate, M.; John, S.; Leonard, S. W.; Lopez, C.; Meseguer, F.; Miguez, H.; Mondia, J. P.; Ozin, G. A.; Toader, O.; van Driel, H. M. *Nature* **2000**, *405*, 437−440.
(35) Stein, A.; Schroden, R. C. *Curr. Opin. Solid State Mater. Sci.* **2001**, *5*, 553−564.
(36) Wang, Z. Y.; Ergang, N. S.; Al-Daous, M. A.; Stein, A. *Chem. Mater.* **2005**, *17*, 6805−6813.
(37) Nichols, J. E.; Cortiella, J. Q.; Lee, J.; Niles, J. A.; Cuddihy, M.; Wang, S. P.; Bielitzki, J.; Cantu, A.; Mlcak, R.; Valdivia, E.; Yancy, R.; McClure, M. L.; Kotov, N. A. *Biomaterials* **2009**, *30*, 1071−1079.
(38) Ha, S. T.; Park, O. O.; Im, S. H. *Macromol. Res.* **2010**, *18*, 935−943.
(39) Choi, S. J.; Yoo, P. J.; Baek, S. J.; Kim, T. W.; Lee, H. H. *J. Am. Chem. Soc.* **2004**, *126*, 7744−7745.
(40) Yoo, P. J.; Choi, S. J.; Kim, J. H.; Suh, D.; Baek, S. J.; Kim, T. W.; Lee, H. H. *Chem. Mater.* **2004**, *16*, 5000−5005.
(41) Holland, B. T.; Blanford, C. F.; Stein, A. *Science* **1998**, *281*, 538−540.
(42) Xia, Y. N.; Gates, B.; Yin, Y. D.; Lu, Y. *Adv. Mater.* **2000**, *12*, 693−713.
(43) Jiang, P.; McFarland, M. J. *J. Am. Chem. Soc.* **2004**, *126*, 13778−13786.
(44) Dimitrov, A. S.; Nagayama, K. *Langmuir* **1996**, *12*, 1303−1311.
(45) Im, S. H.; Park, O. O. *Langmuir* **2002**, *18*, 9642−9646.
(46) Yan, Q. F.; Zhou, Z. C.; Zhao, X. S. *Langmuir* **2005**, *21*, 3158−3164.
(47) Wijnhoven, J. E. G. J.; Bechger, L.; Vos, W. L. *Chem. Mater.* **2001**, *13*, 4486−4499.
(48) Kwak, E. S.; Lee, W.; Park, N. G.; Kim, J.; Lee, H. *Adv. Funct. Mater.* **2009**, *19*, 1093−1099.
(49) Lutkenhaus, J. L.; Hrabak, K. D.; McEnnis, K.; Hammond, P. T. *J. Am. Chem. Soc.* **2005**, *127*, 17228−17234.
(50) Soeno, T.; Inokuchi, K.; Shiratori, S. *Appl. Surf. Sci.* **2004**, *237*, 543−547.
(51) Zhai, L.; Berg, M. C.; Cebeci, F. C.; Kim, Y.; Milwid, J. M.; Rubner, M. F.; Cohen, R. E. *Nano Lett.* **2006**, *6*, 1213−1217.
(52) Dubas, S. T.; Schlenoff, J. B. *Macromolecules* **1999**, *32*, 8153−8160.
(53) Dubas, S. T.; Schlenoff, J. B. *Macromolecules* **2001**, *34*, 3736−3740.
(54) Shiratori, S. S.; Rubner, M. F. *Macromolecules* **2000**, *33*, 4213−4219.
(55) Choi, J.; Rubner, M. F. *Macromolecules* **2005**, *38*, 116−124.
(56) Harris, J. J.; Stair, J. L.; Bruening, M. L. *Chem. Mater.* **2000**, *12*, 1941−1946.
(57) Park, J.; Park, J.; Kim, S. H.; Cho, J.; Bang, J. *J. Mater. Chem.* **2010**, *20*, 2085−2091.
(58) Tettey, K. E.; Yee, M. Q.; Lee, D. *Langmuir* **2010**, *26*, 9974−9980.
(59) Alam, M. N.; Tadasa, K.; Kayahara, H. *Biotechnol. Tech.* **1998**, *12*, 115−118.
(60) Sanli, S.; Altun, Y.; Sanli, N.; Alsancak, G.; Beltran, J. L. *J. Chem. Eng. Data* **2009**, *54*, 3014−3021.
(61) Voinov, M. A.; Kirilyuk, I. A.; Smirnov, A. I. *J. Phys. Chem. B* **2009**, *113*, 3453−3460.
(62) Angelatos, A. S.; Wang, Y. J.; Caruso, F. *Langmuir* **2008**, *24*, 4224−4230.
(63) Park, J.; Hammond, P. T. *Macromolecules* **2005**, *38*, 10542−10550.
(64) Poptoshev, E.; Schoeler, B.; Caruso, F. *Langmuir* **2004**, *20*, 829−834.
(65) Honda, M.; Kataoka, K.; Seki, T.; Takeoka, Y. *Langmuir* **2009**, *25*, 8349−8356.
(66) Wang, X. Y.; Husson, S. M.; Qian, X. H.; Wickramasinghe, S. R. *J. Membr. Sci.* **2010**, *365*, 302−310.
(67) Krasemann, L.; Tieke, B. *Langmuir* **2000**, *16*, 287−290.
(68) Stanton, B. W.; Harris, J. J.; Miller, M. D.; Bruening, M. L. *Langmuir* **2003**, *19*, 7038−7042.
(69) Liu, X. Y.; Bruening, M. L. *Chem. Mater.* **2004**, *16*, 351−357.
(70) Levenstein, R.; Hasson, D.; Semiat, R. *J. Membr. Sci.* **1996**, *116*, 77−92.
(71) Peeters, J. M. M.; Boom, J. P.; Mulder, M. H. V.; Strathmann, H. *J. Membr. Sci.* **1998**, *145*, 199−209.
(72) Lu, O. Y.; Malaisamy, R.; Bruening, M. L. *J. Membr. Sci.* **2008**, *310*, 76−84.
(73) Jin, W. Q.; Toutianoush, A.; Tieke, B. *Langmuir* **2003**, *19*, 2550−2553.
(74) Malaisamy, R.; Bruening, M. L. *Langmuir* **2005**, *21*, 10587−10592.
(75) Hoffmann, K.; Friedrich, T.; Tieke, B. *Polym. Eng. Sci.* **2011**, *51*, 1497−1506.